Supersensitive quantum sensor based on criticality in an antiferromagnetic spinor condensate

Safoura S. Mirkhalaf and Emilia Witkowska*
Institute of Physics PAS, Aleja Lotnikow 32/46, 02-668 Warszawa, Poland

Luca Lepori
Istituto Italiano di Tecnologia, Graphene Labs, Via Morego 30, I-16163 Genova, Italy

(Received 4 December 2019; revised manuscript received 5 March 2020; accepted 9 March 2020; published 14 April 2020)

We consider an antiferromagnetic Bose-Einstein condensate in a transverse magnetic field with a fixed macroscopic magnetization. The system exhibits two different critical behaviors corresponding to transitions from polar to broken-axisymmetry and from antiferromagnetic to broken-axisymmetry phases, depending on the value of the magnetization. We exploit both types of system criticality as a resource in the precise estimation of the control parameter value. We quantify the achievable precision by the quantum Fisher information. We demonstrate supersensitivity and show that the precision scales with the number of atoms up to N^4 around criticality. In addition, we study the precision based on the error-propagation formula, which provides a simple-to-measure signal whose scaling coincides with the quantum Fisher information. Finally, we take into account the effect of nonzero temperature and show that sub-shot-noise sensitivity in the estimation of the control parameter is achievable in the low-temperature limit.

DOI: 10.1103/PhysRevA.101.043609

I. INTRODUCTION

The properties of a system can change dramatically through a small change in a control parameter during a phase transition. Phase transitions can be of a classical or a quantum nature. An example of a classical transition is the ice-water-vapor transition of water in the H_2O system or the ferromagnetic-paramagnetic transition in solid-state materials, with temperature as the external parameter in both cases. On the other hand, quantum phase transitions occur at zero temperature and are induced by a change in a Hamiltonian parameter. Phase transitions are classified according to the basic Ehrenfest classification [1] as first or second order. However, other classifications are also widespread [2]. A first-order phase transition is characterized by the coexistence of two stable phases when the control parameter is within a certain range. On the other hand, a second-order phase transition is characterized by a massless spectrum, inducing power-law scaling for correlations and the notion of universality, which in turn results in a number of critical exponents quantifying how rapidly the system changes around criticality.

At the heart of quantum metrology lies the idea of parameter estimation using a quantum resource. The best precision in the estimation of a particular parameter is quantified by the quantum Fisher information (QFI), related to the distinguishability of a quantum state from a neighbor state in a geometrical space [3]. It is recognized [4] that criticality is considered a perfect resource for parameter estimation. This happens because quantum states around criticality differ greatly from each other, although the control parameter driving the transition varies by only a small amount.

To date, the role of quantum criticality in parameter estimation has been investigated in the Lipkin-Meshkov-Glick [5], Dicke [6,7], bosonic Josephson junction [8], and many other quantum models [9]. The first experiment demonstrating a high sensitivity in parameter estimation around criticality was reported recently for a system composed of condensed atoms in a double-well potential [8]. The majority of these works are devoted to examining the criticality around second-order phase transitions, while only a few concern first-order ones [10–12]. However, due to the much more drastic change in ground-state properties around a first-order transition, it could be interesting to investigate its relevance for control parameter estimation using the states as a quantum resource. Therefore, here we consider a system of a spin-1 Bose-Einstein condensate (BEC) which presents both a first- and a second-order phase transition, depending on the system parameters.

Spinor BECs are composed of N atoms in several Zeeman energy levels with a given hyperfine spin F enumerated by the magnetic number $m_f \in [-F, F]$. Here we concentrate on $F = 1$. The system possesses an additional spin degree of freedom, which leads to a range of phenomena absent in a scalar BEC. The longitudinal magnetization M, which is the difference in the occupations of the $m_f = 1$ vs $m_f = -1$ components, is approximately conserved in the system and acts as an independent external parameter. This conservation law comes from the spin rotational symmetry of contact interactions when dipole-dipole interactions are neglected. The global ground state of the $F = 1$ system is classified as ferro- or antiferromagnetic, depending on the sign of the

*ewitk@ifpan.edu.pl

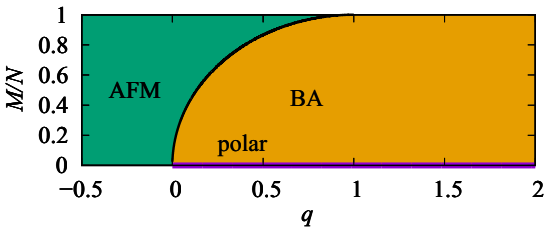

FIG. 1. Mean-field phase diagram of the antiferromagnetic spinor condensate under the single-mode approximation and for fixed magnetization M hosting three phases [16]. In the antiferromagnetic (AMF) phase, the components $m_F = \pm 1$ coexist. In the broken-axisymmetry (BA) phase, atoms occupy all three Zeeman components. In the polar phase, all atoms are in the $m_F = 0$ Zeeman component. In general, the ground state is a superposition of Fock states. However, when $q \ll q_c$, the ground state of the AFM phase is $|(N+M)/2, 0, (N-M)/2\rangle$, while for $q \gg q_c$, the ground state of the BA phase reads $|M, N-M, 0\rangle$. Particularly in the polar phase the ground state is $|0, N, 0\rangle$. The solid black line shows the position of the critical point $q_c = 1 - \sqrt{1-(M/N)^2}$. The quantum phase transition is first order from the polar to the antiferromagnetic phase; it occurs when the magnetization tends to 0. In other cases, the transition from the broken-axisymmetry to the antiferromagnetic phase is of second order.

spin-dependent interactions. The structure of the ground state of a homogeneous system results from the competition between spin-dependent interactions (dominant at low magnetic fields) and the quadratic Zeeman energy (dominant at large magnetic fields), which gives rise to the emergence of two different phases and to a critical point which lies in between them. The position of the critical point depends on the value of magnetization as depicted in Fig. 1. More importantly for the purpose of our work, the order of the phase transition depends on the magnetization value as well. It is first order when the magnetization tends to 0 [13,14] and second order for a macroscopic one [15–17].

The purpose of this paper is to perform a comprehensive study of the metrological usefulness of the two types of criticality appearing in antiferromagnetic condensates. We concentrate on a finite-size system (a few thousand atoms) in which the spatial and internal degrees of freedom can be decoupled. We quantify the metrological usefulness by the quantum Fisher information determined by the fidelity susceptibility [4]. Our numerical method is based on the exact diagonalization of the system Hamiltonian and on the consequent evaluation of the QFI for the ground state. We relate the scaling of the QFI to the critical exponents [9] for macroscopic magnetizations, showing that it scales with the system size as $N^{4/3}$. Our results confirm the general treatment provided in [9]. In the case of zero magnetization, when the phase transition is first order, we found its scaling with the system size to be N^4. We confirmed the numerical results by the analytical perturbative approach. We show that the QFI around the first-order phase transition is much more prominent, at least in the zero-temperature case. In addition, we show that the precision of the estimation of the control parameter can be obtained by using a simple signal, which is introduced as the atomic population in the $m_f = 0$ Zeeman component. Specifically, we evaluate the estimation precision employing the error-propagation formula and confirm that the scaling of its inverse with N coincides with the scaling of the QFI for any magnetization as expected [8]. The extensive use of the error-propagation formula, simpler to obtain than the QFI also in experiments, to estimate the sensitivity of both the first- and the second-order phase transition is one of the central points of the present work. Finally, we consider the effect of a nonzero temperature, showing that the value of the QFI decreases more rapidly for zero magnetization than for a macroscopic one. However, sub-shot-noise scaling of the QFI is still possible when the temperature is lower or of the order of the energy gap.

The paper is organized as follows. In Sec. II, we introduce the model and review the characteristic properties of its phase diagram. In Sec. III, we provide the basics of the estimation theory around criticality. Next, we present our results in detail for zero and nonzero temperatures in Secs. IV and V, respectively. Concluding remarks and a summary are given in Sec. VI.

II. THE SPIN-1 SYSTEM

We consider a spin-1 ($F = 1$) atomic BEC in the presence of a homogeneous transverse magnetic field B. The system is conveniently described by the vector $\vec{\hat{\Psi}} = (\hat{\Psi}_1, \hat{\Psi}_0, \hat{\Psi}_{-1})^T$, whose components correspond to the atoms in the corresponding Zeeman states enumerated by the quantum magnetic number $m_f = 0, \pm 1$. We consider a finite-size system composed of a few thousand atoms in which the generation of spin domains is energetically costly. It is convenient to work under the *single-mode approximation*, in which all atoms in the three Zeeman modes share the same spatial wave function $\phi(\boldsymbol{r})$ [18]. Then the external and internal spin degrees of freedom can be decoupled and the components of the vector are defined as $\hat{\Psi}_{m_f} = \phi(\boldsymbol{r})\hat{a}_{m_f}$, where $\hat{a}_{m_f}$ is the bosonic annihilation operator of an atom in the m_f-th Zeeman state. Consequently, the Hamiltonian is cast in the form [19,20]

$$\frac{\hat{H}(q)}{c} = \frac{1}{2N}\hat{J}^2 - q\hat{N}_0 \tag{1}$$

and consists of two terms: the first one refers to nonlinear contact interactions between pairs of atoms, while the second term shows the effect of a quadratic Zeeman shift on the energy levels. In Eq. (1), $\hat{J}^2$ is the total spin operator, which can be defined in terms of the spin-1 matrices (see Appendix A), $\hat{N}_{m_f}$ is the occupation number operator of atoms in the m_f Zeeman state, the total atom number N is the eigenvalue of $\hat{N} = \sum_{m_f} \hat{N}_{m_f}$, and $c = Nc_2 \int d\boldsymbol{r}|\phi(\boldsymbol{r})|^4$, with the spin-dependent interaction coefficient c_2 defined in terms of the s-wave scattering lengths [21]. The positive (negative) sign of c represents the antiferromagnetic (ferromagnetic) nature of interactions [18]. The coupling constant q gives the strength of the quadratic Zeeman energy. In fact, the parameter q can be the sum of two terms, $q = q_B + q_M$, as it can be changed using the magnetic and off-resonant microwave dressing fields, denoted q_B and q_M, respectively [15,16]. The value of q can therefore be tuned between negative and positive values.

The Hamiltonian, (1), preserves the z component of the total spin operator, $\hat{J}_z = \hat{N}_{+1} - \hat{N}_{-1}$, due to $[\hat{H}, \hat{J}_z] = 0$. Therefore, the eigenvalues of $\hat{J}_z$, which are $M = -N, -N+1, \ldots, N$, being the magnetization, can be used to label the Hamiltonian eigenbasis (more details in Appendix A). This is justified based on the fact that the spin-dependent interaction has rotational symmetry as long as the spin-1 system is isolated from its environment and dipolar interactions are neglected [17]. This is also the main reason why the linear Zeeman energy plays no role in the Hamiltonian, (1), and it acts only as a constant shift on the energy levels.

Our numerical method is based on the exact diagonalization of Hamiltonian (1) and is described in detail in Appendix B. For convenience, we consider even values of N, nonnegative values of M, and antiferromagnetic interactions ($c > 0$), which can be realized with a condensate of sodium-23 atoms in the $F = 1$ or $F = 2$ manifold. For the case of trapping atoms in a flat trap of volume V, we can assume a homogeneous density for the condensate, such that $\phi(\boldsymbol{r}) = \frac{1}{\sqrt{V}}$. Consequently, $c = c_2 \frac{N}{V}$. Here, $\frac{N}{V}$ is the density of the system, which is maintained as a fixed parameter. In the following, we use c as the energy unit.

It has been discussed in the literature that Hamiltonian (1) exhibits both first- and second-order phase transitions at critical values of the external parameter q [18,22]. In particular, for the case of zero magnetization, the transition occurs between the longitudinal polar and the broken-axisymmetry phases, while in the case of macroscopic magnetization the transition is between the antiferromagnetic and the broken-axisymmetry ones. We provide the characteristics of particular phases and expressions for the corresponding ground states in the caption to Fig. 1. Moreover, using the fractional occupation number in the $m_f = 0$ state $n_0 = \langle \hat{N}_0 \rangle / N$ as the order parameter, one can define the critical value of q as $q_c = 1 - \sqrt{1 - (M/N)^2}$ for a given M/N in the thermodynamic limit using the mean-field approach [23]. The corresponding phase diagram of the antiferromagnetic condensate has been explored experimentally [15–17] and agreement with theoretical predictions has been noted.

In many-body systems in the thermodynamic limit, an abrupt continuous (discontinuous) change in the first derivative of the ground-state energy (at zero temperature) around criticality is observed. This behavior marks a continuous second-order (discontinuous first-order) phase transition. A radical change in the derivative of the ground-state energy E_0 is also linked to abrupt changes in the order parameter based on the Hellmann-Feynman theorem, which gives $n_0 \equiv -\langle \frac{1}{N} \frac{\partial \hat{H}(q)}{\partial q} \rangle = -\frac{1}{N} \frac{\partial E_0(q)}{\partial q}$ [24] upon consideration of our Hamiltonian, (1). In Fig. 2 we show variations of the first (upper panel) and of the second (lower panel) derivatives of the ground-state energy of Hamiltonian (1) for finite-size systems with $N = 1000$ and 4000. In the case of macroscopic magnetization (right column) the first derivative of the ground state changes continuously while the second derivative of the energy exhibits an abrupt but continuous change around criticality. The second derivative shows discontinuous behavior in the thermodynamic limit. On the other hand, for zero magnetization, the first derivative of E_0 shows a continuous but sudden

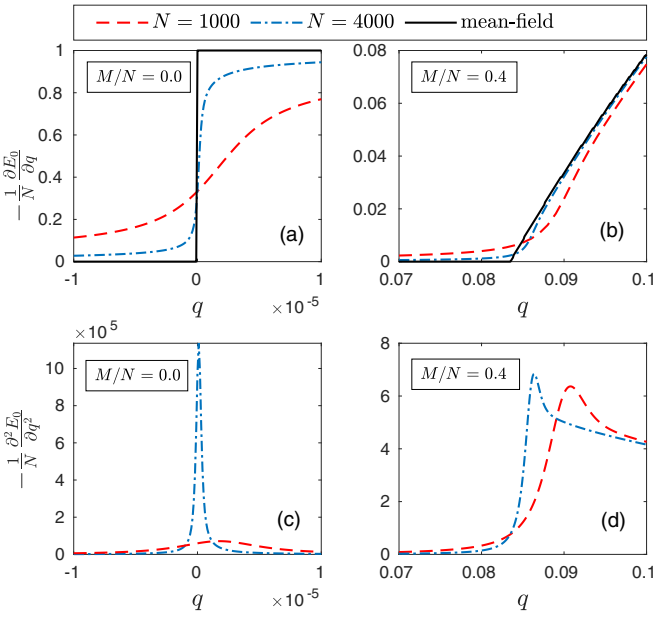

FIG. 2. Upper panel: First derivative of the ground-state energy of Hamiltonian (1) versus q obtained numerically using the exact diagonalization method for $N = 1000$ (dash-dotted blue line) and $N = 4000$ (dashed red line), compared to the mean-field results (solid black line). Lower panel: Second derivative of the ground-state energy versus q for the same parameters. Left and right columns correspond to $M/N = 0$ and $M/N = 0.4$, respectively.

variation (left column). This variation trends to a discontinuity when approaching the thermodynamic limit. The peak of the second derivative of energy is greatly sharpened around criticality. It is noteworthy that for $M = 0$ and $q \sim 0$ the ground state gives $\langle \hat{N}_0 \rangle = N/3$ [25]. In this case, all higher-order derivatives of the ground-state energies are discontinuous. In general, we conclude that quantum phase transitions are quite smooth, due to the finite sizes of the considered system. While the mean field works in the thermodynamic limit, for typical ultracold gas experiments with average-sized ensembles, the mean-field results do not necessarily hold. In this case, the variation of population observables (such as n_0's) should be extracted in the full quantum approach [17]. For a finite-size condensate of N spin-1 atoms, the value of q_c depends on the ratio M/N and c, at least to some extent. In order to drive the system throughout the critical region one can tune the control parameter q with an external magnetic field or microwave dressing from negative to positive values. This can be used to estimate the value of q.

Indeed, it has been discussed that the family of quantum states around a critical point can be used as a resource for quantum sensing [4]. This is possible because a small variation in the control parameter around criticality leads to a remarkable change in the properties of these states. In the following, we analyze both types of criticality in an antiferromagnetic spin-1 system and show that the precision of the estimation of the coupling constant q is greatly enhanced compared to that in noncritical regions. To this end, in the next section we briefly present the relation between criticality and metrology. In this spirit, we describe the quantum Fisher

information as the essential parameter which provides a bridge between these territories.

III. QUANTUM ESTIMATION THEORY AROUND CRITICALITY

A quantum phase transition concerns a radical change in the ground states of a particular Hamiltonian at a specific critical point. It has been proved [4] that while varying a control parameter drives the system into different phases, this can be used to enhance the precision of the estimation of the control parameter by its own. This means that criticality can be a resource in quantum metrology. Here, we recall the main ingredients of the critical metrology formalism, which is based on the definition of the QFI.

Let us consider the generic Hamiltonian form

$$\hat{H}(q) = \hat{H}_0 + q\hat{H}_q, \tag{2}$$

whose ground state $|\psi_0(q)\rangle$ exhibits a quantum phase transition at a critical value of $q = q_c$ (at zero temperature). This means that the ground state of the above Hamiltonian shows a drastic change, varying from $|\psi_0(q)\rangle$ to $|\psi_0(q+\delta_q)\rangle$ for a small variation in δ_q around the quantum critical point (QCP) at q_c. The physical quantity that is used to evaluate the difference between the two pure quantum states, including the ground state, is defined by the fidelity [26],

$$\mathcal{F} = |\langle\psi_0(q)|\psi_0(q+\delta_q)\rangle|. \tag{3}$$

The relation between the fidelity and the quantum Fisher information F_q is [3,27–29]

$$F_q = -4\frac{\partial^2\mathcal{F}}{\partial{\delta_q}^2}\bigg|_{\delta_q=0}. \tag{4}$$

More explicitly [4],

$$F_q(|\psi_0(q)\rangle) = 4[\langle\partial_q\psi_0|\partial_q\psi_0\rangle - |\langle\partial_q\psi_0|\psi_0\rangle|^2] \tag{5}$$

$$= 4\sum_{n\neq 0}\frac{|\langle\psi_0|\hat{H}_q|\psi_n\rangle|^2}{(E_0-E_n)^2}. \tag{6}$$

Here, $|\psi_n\rangle$ and E_n refer to the nth excited eigenstates and eigenvalues of (2), respectively, and $\partial_q \equiv \partial/\partial q$. Moreover, Eq. (5) can be obtained by Taylor expanding the state $|\psi_0(q+\delta_q)\rangle$ around $|\psi_0\rangle$ up to second order in δ_q and excluding the first derivate term due to the normalization condition, $\partial\langle\psi_0|\psi_0\rangle/\partial q = 0$ [30].

It is important to note that formula (5) is valid if the first derivative of the ground state exists. In the case of the first-order quantum phase transition, due to the level crossing the first derivative of the ground state is discontinuous. However, in this work, we focus on a finite-size system and therefore the level crossing changes to avoided level crossing. As a result, definition (5) is still valid in the case of the first-order phase transition [31]. In addition, as discussed in [7] and [32], the QFI and the Bures metric correspondence are not broken provided that the rank of the ground-state density matrix is not changed in the critical region [33]. This also works in our case where the quantum state of the system remains pure, with rank 1 for zero temperature and rank 2 in the finite-temperature case [7,32].

The QFI is related to the geometrical distinguishability of quantum states separated by a small variation in q. Consequently, its value is significantly increased around criticality. This is easily observed from the QFI, (6), since one of the excited eigenvalues approaches the ground state at the QCP [4]. On the other hand, the QFI is connected to the precision of the estimation of the q parameter. In (2), one may consider the unknown coupling constant as an imprinted phase to be measured [9]. Since there is no direct observable corresponding to the coupling constants, we cannot measure its value by just using the conventional approach in quantum mechanics, that is, evaluating the expectation value of an observable in a particular state. Therefore, the problem of measuring q becomes an estimation problem [34]. The ultimate bound of estimation, called the quantum Cramer-Rao bound (QCRB), is set by the inverse of the QFI:

$$\delta q^2 \geqslant \delta q^2_{\mathrm{QCRB}} = \frac{1}{F_q}. \tag{7}$$

Therefore, the precision of the estimation of q is significantly improved at criticality, implying that it is a resource in estimation theory [4,30].

In the case of mixed states $\hat{\rho}(q) = \sum_n w_n|\psi_n\rangle\langle\psi_n|$, the fidelity, (3), is replaced by the more general definition [26,35]

$$\mathcal{F} = \mathrm{tr}[\sqrt{\hat{\rho}(q)}\hat{\rho}(q+\delta_q)\sqrt{\hat{\rho}(q)}]^{1/2}, \tag{8}$$

which can still be exploited, by using (4), to obtain the QFI. The explicit result for a single-parameter estimation is [34,36]

$$F_q = 2\sum_{n,m}\frac{|\langle\psi_n|\partial_q\hat{\rho}_q|\psi_m\rangle|^2}{w_n+w_m} \tag{9}$$

for a finite number of particles and continuous phase transition [36].

As mentioned before, the QFI gives the upper bound of the sensitivity. However, it is not always easy to find the optimal measurement to saturate the QCRB. Moreover, it is not straightforward to extract the QFI experimentally. This refers to the fact that, in practice, in order to find the QFI, one needs the full tomography of $\hat{\rho}(q)$ and $\hat{\rho}(q+\delta_q)$. This process is not easy to implement in large systems. Therefore, it is convenient to consider the precision given by the error-propagation formula defined as the signal-to-noise ratio [9],

$$\delta q^2 = \frac{\Delta^2\hat{\mathcal{S}}}{|\partial_q\langle\hat{\mathcal{S}}\rangle|^2}, \tag{10}$$

where the variance in the signal $\hat{\mathcal{S}}$ is given by $\Delta^2\hat{\mathcal{S}} = \langle\hat{\mathcal{S}}^2\rangle - \langle\hat{\mathcal{S}}\rangle^2$. The signal does not always saturate the upper bound of sensitivity, (7). Nevertheless, it has the advantage of being easier to measure in realistic experiments. On the other hand, having access to the error-propagation formula, (10), only requires the first and second moments of the signal (i.e. $\langle\hat{\mathcal{S}}\rangle$ and $\langle\hat{\mathcal{S}}^2\rangle$, respectively).

The upper bound for the scaling of the above-introduced QFI is set by critical exponents for the second-order quantum phase transition. It was shown that $F_q \propto N^\mu$, where $\mu = 2/(d\nu)$, with ν the critical exponent satisfying the divergence of the correlation length and d the effective spatial dimension, as explained in [8] and [9]. No bound is expected for the scaling exponent of the QFI around the first-order quantum phase

transition. On the other hand, the standard quantum limit is equal to the total atom number N in the zero-temperature case. In addition, we point out that the QFI in (4), where the states entering into the fidelity are separated by a variation in q, is a different quantity from that defined in quantum interferometry, where states are linked by a unitary operation [37]. Notably, only the QFI defined in the second way, G, demonstrates multipartite entanglement and subject to the Heisenberg limit for its scaling with the number of particles N, i.e., $G(N) \sim N^{\zeta}$, $\zeta \leqslant 2$ [37,38].

IV. PRECISE ESTIMATION AROUND CRITICALITY

The antiferromagnetic spin-1 system exhibits two types of criticalities, depending on the value of the magnetization and characterized by different behaviors of the second derivative of the ground-state energy, as mentioned in Sec. II. In the following, we exploit the quantum criticalities of a spin-1 antiferromagnetic condensate in a transverse magnetic field to demonstrate a high sensitivity of the estimation of the coupling constant q using the QFI formalism introduced above. We also provide the useful experimental signal $\hat{\mathcal{S}}$, which almost saturates the QCRB.

A. Zero magnetization

Let us consider first the case of $M = 0$, where the system shows a discontinuous quantum phase transition in the thermodynamic limit with the critical point at $q_c = 0$ [23]. The variation of F_q, defined as (6), versus q for $N = 1000$ is shown in Fig. 3. Obviously, the value of F_q increases significantly around criticality, dropping down far away from the critical region. We also show in the same figure the sensitivity estimated by the error-propagation formula, (10), when the signal is set to the number of atoms in the $m_f = 0$ Zeeman state, $\hat{\mathcal{S}} = \hat{N}_0$. The inverse of (10) almost saturates the QFI, and we observe the same behavior for both quantities when increasing the precision around criticality. Note that the maxima of F_q and $1/\delta q^2$ are shifted to the same extent with respect to the mean-field critical point $q_c = 0$ due to the finite number of atoms considered. That is, upon increasing N, the evaluated q_c value for a finite system approaches the prediction of the mean-field formalism for $N \to \infty$ [23].

In order to see how the total number of atoms affects the precision in the inset in Fig. 3, we show the logarithms of the maxima of F_q and $1/\delta q^2(\hat{N}_0)$ versus $\log N$. Both of them exhibit exponential behavior. The fitting gives the same scaling exponents for the QFI and for the inverse $1/\delta q^2$, i.e., $F_q^{\max} \sim [1/\delta q^2]^{\max} \sim 0.05N^4$, which beats the sub-shot-noise sensitivity $\sim N$. The identification of the particular signal that saturates the QFI is important from the experimental point of view. The reason is that in order to find the QFI, one needs to determine the full tomography of the density matrix and subsequently to evaluate the QFI, (8), which is hardly possible for large systems, as mentioned before. Alternatively, one may extract the classical Fisher information, i.e., $F_c = \sum_x (\partial_q P(x|q))^2/P(x|q)$, where $P(x|q)$ is the probability distribution of getting q conditioned on making measurements over all eigenvalues of an observable $\hat{X}$, $(\hat{X}|x\rangle = x|x\rangle)$ [39]. The optimization of the classical Fisher information over all possible observables approaches the QCRB marked by the QFI. On the other hand, measurement of the number of atoms in the $m_f = 0$ Zeeman component and extraction of its first and second moments are more easily accessible in practice and yet provide essentially the same information.

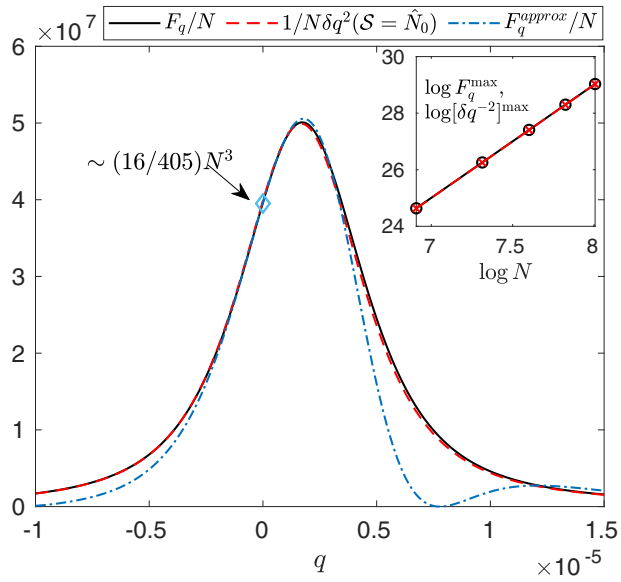

FIG. 3. The scaled quantum Fisher information F_q/N (solid black line), the precision $1/N\delta q^2$ (dashed red line), and the analytical F_q^{approx}/N results up to the second correction using perturbation theory around $q \sim 0$ (dash-dotted blue line) versus the parameter q for $N = 1000$ and $M/N = 0$. The turquoise diamond marks the explicit analytical value of the QFI at $q = 0$, i.e., $F_q(q = 0)/N = (16/405)N^3$. Note that the perturbation theory prediction is in good agreement with the F_q in the validity range of the perturbative approach, that is, for small enough q. Inset: Logarithm of the maxima for F_q and $1/\delta q^2$ $(\hat{\mathcal{S}} = \hat{N}_0)$ depending on $\log N$.

As the region of criticality is around $q = 0$, when the magnetization is 0, it is convenient to use the perturbation theory to approximate the eigenvalues and eigenvectors of Hamiltonian (1). Using these, it is possible to approximate the QFI value around criticality and to extract the corresponding scaling exponent. To this end, we employ the second-order perturbation theory formalism for small values of q. Suppose that the unperturbed Schrödinger equation (with $q = 0$) has $\hat{H}_0|\psi_n^{(0)}\rangle = E_n^{(0)}|\psi_n^{(0)}\rangle$. When the parameter q is small but nonzero, the idea is to express the Schrödinger equation $(\hat{H}_0 + q\hat{H}_q)|\tilde{\psi}_n\rangle = \tilde{E}_n|\tilde{\psi}_n\rangle$ up to the second-order corrections

$$\begin{aligned} \tilde{E}_n &= E_n^{(0)} + qE_n^{(1)} + q^2E_n^{(2)} + O(q^3), \\ |\tilde{\psi}_n\rangle &= |\psi_n^{(0)}\rangle + q|\psi_n^{(1)}\rangle + q^2|\psi_n^{(2)}\rangle + O(q^3), \end{aligned} \tag{11}$$

where every single term can be expressed by the eigenvalues and eigenstates of the unperturbed Hamiltonian $\hat{H}_0$ [40]. Consequently, one can find the explicit corrections to the eigenenergies $\tilde{E}_n^{(1,2)}$ and eigenstates $|\psi_n^{(1,2)}\rangle$ of the spin-1 system when $\hat{H}_0 = \frac{c}{2N}\hat{f}^2$ and $\hat{H}_q = -\hat{N}_0$. More details on the derivation of the results are presented in Appendix C [see Eqs. (C3) and (C4)]. In Fig. 3 we show the QFI calculated using expression (6) and approximated eigenvalues and eigenstates. Agreement between the exact results and those

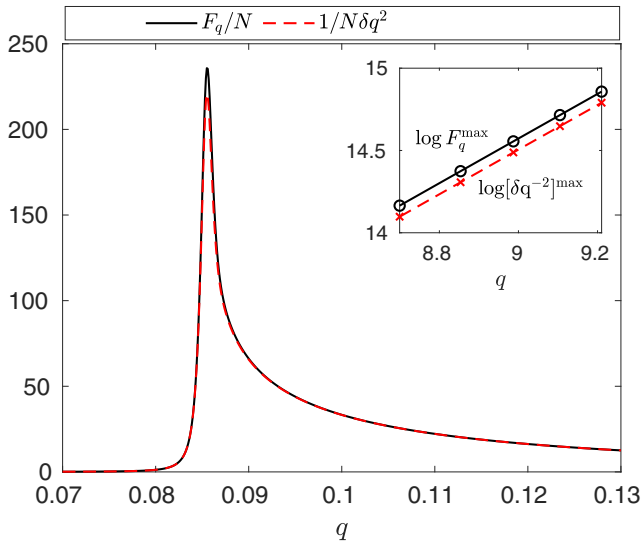

FIG. 4. Scaled quantum Fisher information F_q/N (solid black line) and scaled precision $1/(N\delta q^2)$ calculated with $\hat{\mathcal{S}} = \hat{N}_0$ (dashed red line) versus q for $N = 6000$ and $M/N = 0.4$. Here, the critical point is shifted compared to the one given by the mean field at $q_c = 0.084$. Inset: Logarithm of the maxima for F_q and $1/\delta q^2$ ($\hat{\mathcal{S}} = \hat{N}_0$) versus N.

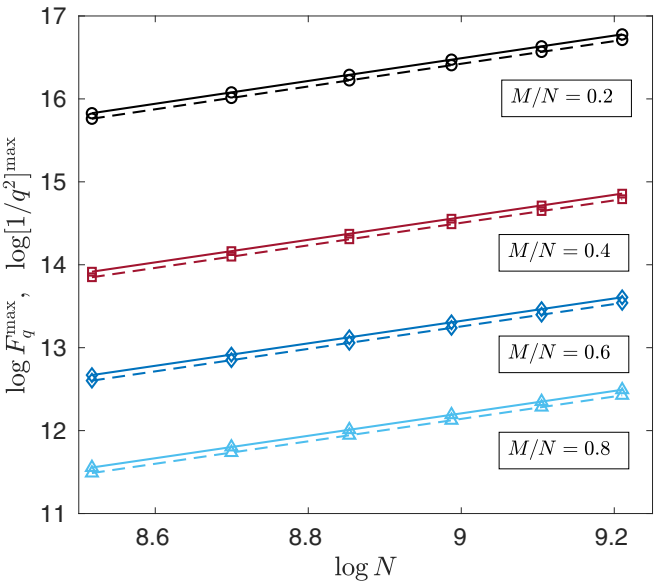

FIG. 5. Logarithm of the maxima for F_q (solid lines) and for $1/\delta q^2$ (dashed lines) versus $\log N$ for different values of M/N: 0.2, 0.4, 0.6, and 0.8. The values of both maxima increase with the number of particles N and follow the power law $F_q^{\max} \propto N^{\mu}$ ($[1/\delta q^2]^{\max} \propto N^{\mu'}$) with fixed μ (μ').

approximated by the perturbation theory is found when $q \sim 0$. The value of the QFI can be calculated analytically at $q = 0$ using the approximated eigenstates and eigenvectors, (C3) and (C4). We found that $F_q(q = 0) \approx N^3(N + 3)16/405$, which is $\propto 0.04N^4$. This result is in excellent agreement with the numerical prediction for the QFI value as demonstrated in Fig. 3. To this purpose, one may also consider the ratio $1/\delta q^2$ with the signal $\hat{\mathcal{S}} = \hat{N}_0$ by inserting the approximated ground state, (C3), into (10). We obtain $1/\delta q^2 = \frac{16}{405}N^4$ for small q using the first- and second-order moments of $\hat{N}_0$ and (B11). This result is in complete agreement with the approximated QFI value.

Finally, we note that for a second-order quantum phase transition an algebraic scaling for the QFI is expected [41], similarly as for the relevant observables (see, e.g., [42]). This behavior is implied by scale invariance, in turn allowed by the vanishing of the mass gap in the thermodynamic limit. On the contrary, at a first-order quantum phase transition, the same scalings can occur only provided that the correlation length (of the order of the inverse of the mass gap) is at least equal to the finite size of the considered system. A similar situation occurs, for instance, for two points connected correlations. For both types of quantum phase transition, algebraic ansatzes for the scalings of the observables can be adopted for finite-size analysis.

B. Macroscopic magnetization

When the magnetization is nonzero, a continuous quantum phase transition occurs in the system as discussed in Sec. III. In this case, the position of the critical point is $q_c = 1 - \sqrt{1 - (M/N)^2}$ as shown by the mean-field approach [23]. The variations of the QFI and of the inverse of the signal-to-noise ratio for $\hat{\mathcal{S}} = \hat{N}_0$ versus q are shown in Fig. 4 using $N = 6000$ and $M/N = 0.4$. Similarly to the case of zero magnetization, the values of F_q and $1/\delta q^2$ increase significantly around criticality. We extracted the scaling of the maxima of the QFI and of $1/\delta q^2$. We show its logarithms versus $\log N$ in the inset in Fig. 4. We obtained $F_q^{\max} \sim 10.7N^{1.36}$ and $[1/\delta q^2]^{\max} \sim 10.05N^{1.36}$, which have the same power-law scaling versus N with different prefactors. In the case of macroscopic magnetization we observe $F_q \sim N^{4/3}$. This means that $\mu = 4/3$.

The agreement between the scaling exponents of the QFI and of $1/\delta q^2$ has been generally demonstrated to occur at second-order quantum phase transitions, provided that the signal coincides with the order parameter [8]. In the same paper this equivalence was measured explicitly for a bosonic Josephson junction model realized in an ultracold atom setup. It is interesting that the same agreement arises in our model at the first-order transition, perhaps due to the appearance of a scaling regime at the considered finite sizes. It is also noteworthy that the scaling exponent that we found here gives the same scaling as for the QFI (or, equivalently, the fidelity susceptibility) in the Lipkin-Meshkov-Glick [43], Dicke [44], and bosonic Josephson junction [8] models.

In order to demonstrate how increasing the magnetization changes the estimation precision, in Fig. 5 we show the maximum values for the QFI and for $1/\delta q^2$, versus $\log N$ for different values of M/N. The maximum value of $\log F_q$ grows upon increasing the number of particles for different values of the fractional magnetization. Moreover, by increasing M/N, the maximal values of the QFI decrease while they still display very similar slopes. This suggests that the scaling of the QFI with N can have the same scaling power law with the same scaling exponent:

$$F_q^{\max} \propto N^{\mu}. \tag{12}$$

TABLE I. Values of the scaling exponent for the maxima of the quantum Fisher information $F_q^{\max} \propto N^{\mu}$, for the inverse of the error-propagation formula $[1/\delta q]^{\max} \propto N^{\mu'}$, and for the energy gap $\Delta_N^{\min} \propto N^{\alpha}$ versus the fractional magnetization M/N. Here, the values are extracted by fitting to the numerical data.

	M/N			
	0.2	0.4	0.6	0.8
μ	1.37	1.36	1.35	1.35
μ'	1.37	1.36	1.35	1.35
α	−0.35	−0.34	−0.34	−0.34

To be more precise, in Table I we list the scaling exponents for each of the lines shown in Fig. 5 versus the fractional magnetization M/N. The value of μ is almost fixed for different values of the fractional magnetization M/N. In addition, a similar behavior is observed for $1/\delta q^2$, $[1/\delta q^2]^{\max} \propto N^{\mu'}$. We discuss this point in more detail in Sec. VI.

Thus far, we have considered the effect of criticality in the ideal case of zero temperature. Nevertheless, in realistic situations the temperature is always above absolute zero and the system, (1), is never in a pure state but, rather, in mixed states. Motivated by this fact, in the following section we consider the effect of a finite temperature on the estimation precision.

V. THE ROLE OF NONZERO TEMPERATURE

In the case of a nonzero temperature T, the quantum states of the system are described by the canonical Gibbs density matrix

$$\rho(q) = \sum_n \frac{e^{-E_n(q)/k_BT}}{Z} |\psi_n\rangle\langle\psi_n|, \tag{13}$$

where the eigenstates are weighted by $w_n := e^{-E_n(q)/k_BT}/Z$ and $Z := \mathrm{tr}(e^{-H/k_BT})$ is the partition function with the Boltzmann constant k_B. The QFI and the signal-to-noise ratio can be extracted using Eqs. (8) and (3) [45]. We focus on the case of macroscopic magnetizations here and return to zero magnetization later. In Fig. 6, we provide the density plots of F_q (a) and $1/\delta q^2$ (b) versus q and k_BT for $N = 100$ and $M/N = 0.4$. As the temperature is increased, the maximum value of F_q and $1/\delta q^2$ approaches 0. For the case of zero magnetization, we have obtained the same qualitative plots as for macroscopic magnetization, given in Fig. 6. However, the region where the QFI and $1/\delta q^2$ are not affected by temperature is pushed toward the lower temperature range.

In order to understand the finite-temperature behavior, let us first investigate the energy gap $\Delta(q, N) = E_0(q) - E_1(q)$, defined as the energy difference between the ground state and the first excited state of the Hamiltonian, (1), close to criticality. The minimum of the energy gap is expected to be subject to the asymptotic law [47,48]

$$\Delta_{\min} \propto N^{\alpha}, \tag{14}$$

and its variation to a scaling function of the form

$$\Delta(N, q) = \Delta_{\min} f(N^{\beta}\epsilon), \tag{15}$$

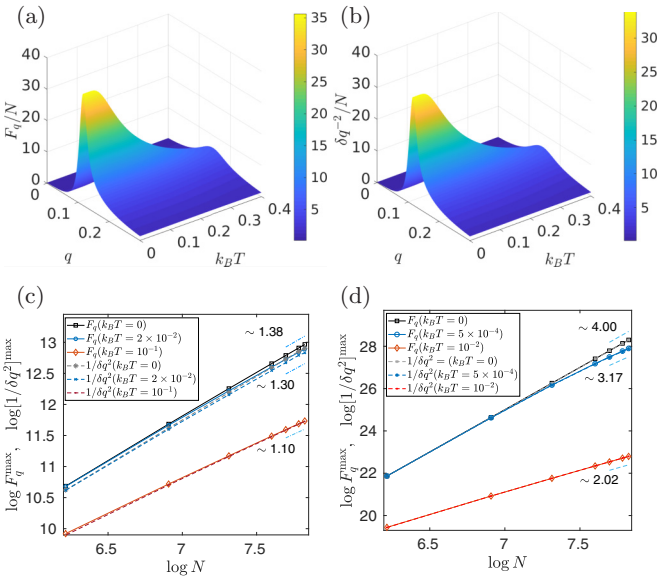

FIG. 6. The precision in the estimation of the parameter q quantified by F_q (a) and the error-propagation formula through $1/\delta q^2$ (b) versus q and k_BT for $N = 100$ and $M/N = 0.4$. The estimation precision decreases with an increase in the temperature. This is due to the increasing thermal fluctuations, which beat the quantum effects. Logarithms of the maximal values for F_q (solid lines) and $1/\delta q^2$ (dashed lines) versus $\log N$ for $k_BT/c = 0,\ 2 \times 10^{-2}$, and 10^{-1} when $M/N = 0.4$ (c) and $k_BT/c = 0,\ 5 \times 10^{-4}$, and 10^{-2} when $M/N = 0$ (d). The sensitivity of the estimation of q approaches the standard quantum limit for both the QFI and $1/\delta q^2$ when the temperature increases. In the case of zero magnetization (d), a change in the value of the scaling exponent is observed for the lowest temperature ($k_BT/c = 5 \times 10^{-4}$). A few points on the right-hand side of the blue curve lie in the intermediate regime, where the scaling exponent is modified due to the nonzero temperature, because their corresponding energy gaps are of the order of the temperature.

where $f(x)$ is the homogeneous function and $\epsilon = q - q_c^N$, with q_c^N being the position of the energy gap minimum. The scaling exponents α and β are independent of the system size, and moreover, they are the same for all systems belonging to the same universality class. We verified the energy gap scaling and we demonstrate it for $M/N = 0.4$ in Fig. 7(a).

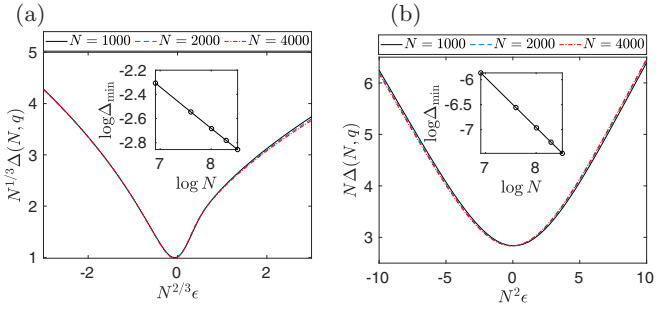

FIG. 7. Scaling of the energy gap, (15), for (a) $M/N = 0.4$ and (b) $M = 0$. Inset: Logarithms of the energy gap minimum versus $\log N$. The fits confirm the power-law behavior, (14), with the scaling exponents $\alpha = -0.34$ for $M/N = 0.4$ and $\alpha = -1$ for $M = 0$.

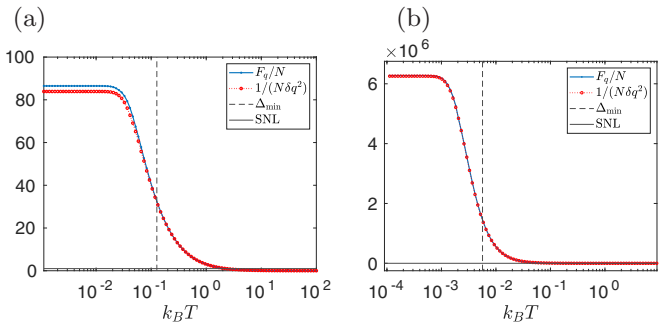

FIG. 8. Decay of the maximal values of the QFI and of $1/\delta q^2$ in the presence of a nonzero-temperature k_BT for $N = 500$ and (a) $M/N = 0.4$ and (b) $M = 0$. The dashed vertical line marks the value of the energy gap, while the solid black line marks the zero-temperature limit. When the temperature is of the order of the energy gap, one can still obtain the sub-shot-noise sensitivity.

In addition, in the inset in Fig. 7(a), we provide the values for the fitted scaling exponent and show that it scales as $\Delta_{\min} \propto N^{-0.34}$ for macroscopic magnetization $M/N = 0.4$. In Table I, we list the scaling exponents of the energy gap minimum α versus other values of the fractional magnetization M/N; all of them are close to $-1/3$. Our findings are consistent with the prediction for an antiferromagnetic condensate [15]. Moreover, the scaling exponent of the energy gap is the same as that for a ferromagnetic spinor condensate [20], the Lipkin-Meshkov-Glick [48], the bosonic Josephson junction [8], and the interacting Dicke [47] models. In the case of zero magnetization the energy gap minimum scales as N^{-1} [15,49,50]. Although the universal behavior cannot be expressed in terms of critical exponents, it indeed can be observed in Fig. 7(b) with the scaling of the energy gap minimum as $\Delta_{\min} = 2.83N^{-1}$.

Having explored the energy gap of the system, we can now achieve a better understanding of the finite-temperature behavior of both F_q and $1/\delta q^2$. We demonstrate this for the macroscopic $M = 0.4$ in Fig. 8(a) and zero magnetization in Fig. 8(b). Three regimes of the QFI (and $1/\delta q^2$) can be distinguished, depending on the temperature value compared to the energy gap: (i) the quantum (zero-temperature) regime for $k_BT \ll \Delta_{\min}$; (ii) the intermediate regime, when $k_BT \approx \Delta_{\min}$; and (iii) the classical regime for $k_BT \gg \Delta_{\min}$ [51–53]. In the first regime, F_q and $1/\delta q^2$ are robust against thermal fluctuations. However, as the temperature increases, both the QFI and $1/\delta q^2$ decrease. In the third regime, the scaling of the QFI approaches the classical shot-noise limit, which is $\sim N$. Moreover, it is interesting to note that in the case of the first-order phase transition the quantum robust regime is pushed toward lower temperatures compared to that of the second-order phase transition. This is due to the fact that in the latter case, the (finite-size) energy gap is three times smaller than the second-order one [15]. This squeezes the quantum robust regime to lower temperatures in the case of zero magnetization.

To investigate the effect of a finite temperature more quantitatively, in Fig. 6 we show the corresponding logarithmic values of $F_q^{\max}$ and $[1/\delta q^2]^{\max}$ versus $\log N$, changing the temperature from 0 to $k_BT/c = 2 \times 10^{-2}$, 10^{-1} for the magnetization $M/N = 0.4$ [Fig. 6(c)] and to $k_BT/c = 0.0005$, 0.01 for zero magnetization [Fig. 6(d)]. As we show, for large enough values of N and macroscopic magnetization, the scaling exponent for the maximum value of the QFI is reduced from 1.38 for zero temperature to 1.30 for $k_BT = 0.02$ and, further, to 1.1 close to the shot-noise limit. A decrease in the scaling exponent also occurs for zero magnetization when it changes through 3.17 ($k_BT/c = 5 \times 10^{-4}$) and 2.02 ($k_BT/c = 10^{-2}$), approaching the shot-noise limit for higher temperatures.

VI. DISCUSSION AND CONCLUSION

In the previous sections, we have discussed the effect of criticality in a spin-1 BEC located in a transverse magnetic field in order to estimate the value of the coupling constant. We have reported that the precision of the estimation of q depends on the type (nature) of criticality we employ.

To this end, we have made use of the quantum Fisher information as a theoretical criterion to estimate the sensitivity of our spinor sensors around the critical region. In addition, we have considered the sensitivity evaluated using the error-propagation formula. We introduced the respective signal (equivalent to the population in the $m_f = 0$ manifold, i.e., $\hat{\mathcal{S}} = \hat{N}_0$). The identification of this simple-to-measure signal and the error-propagation formula is of experimental importance, as it contains the variance $\Delta^2\hat{N}_0$ and the average population $\langle\hat{N}_0\rangle$, which makes it possible to find the sensitivity much more easily than by the QFI measurement. Indeed, evaluating the QFI requires state tomography of the system density matrix $\hat{\rho}$, which would be a challenging task for ensembles consisting of thousands of atoms.

First, we have shown that a first-order quantum phase transition is realized for zero magnetization in the system, when the transition from the polar to the antiferromagnetic phase occurs. For a finite-size spinor condensate with total number of atoms N, we have found that the QFI and the inverse of the signal-to-noise ratio $1/\delta q^2$ scale $\propto N^4$. We also investigated the behavior of the QFI around the transition between the antiferromagnetic and the broken-axisymmetry phases which occurs for macroscopic magnetization. In this case, we calculated the scaling of the QFI versus N as $F_q \sim N^{4/3}$ around the critical point. We evaluated the same scaling factors for $1/\delta q^2$, finding the same qualitative behavior as for the QFI. The reason for the decreasing sensitivity with increasing magnetization lies in the fact that the quantum Fisher information is related to the distinguishability of the quantum states of the different phases around the critical points.

The scaling observed by us can also be analyzed in a different way. As we show in Fig. 2, the ground state exhibits a much more pronounced change around criticality in the case of zero magnetization. In order to get a physical sense, we consider the error-propagation formula, (10). In this regard, one can show that in the zero-magnetization case, where the first-order quantum phase transition occurs, both the variance $\Delta^2\hat{N}_0$ and the slope of the zero-manifold population $\langle\hat{N}_0\rangle$, dependent on q, are maximized. In particular, at the critical point, the variance of $\hat{N}_0$ scales $\propto N^2$ [17], while $\partial_q\langle\hat{N}_0\rangle \propto N^3$ (see Appendix A for explicit expressions). As a result, δq^2

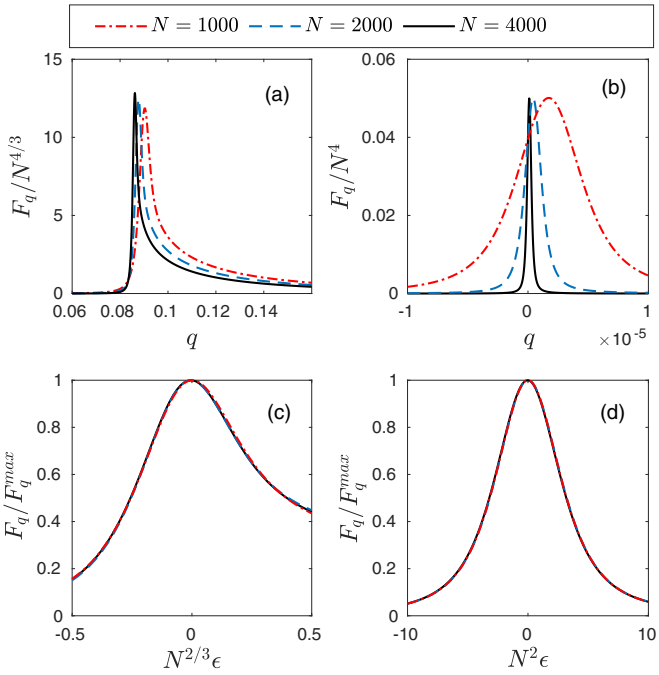

FIG. 9. Upper panel: Scaling of the quantum Fisher information, (16), for (a) $M/N = 0.4$ and (b) $M = 0$ and for different values of the total atomic number N. Lower panel: Universal behavior of the QFI versus the dimensionless parameter $\epsilon = q - q_c^N$ for the same magnetization values.

scales as N^4 around criticality. On the other hand, in the nonzero magnetization case, hosting the second-order phase transition, it is not the variance $\Delta^2\hat{N}_0$ which is maximized around the critical point; rather, its slope $\partial_q(\Delta^2\hat{N}_0)$ is maximized quite close to q_c. Nevertheless, the denominator $\partial_q\langle\hat{N}_0\rangle$ still increases around the QCP. As a result, in the second-order phase transition, the interplay of the nominator and denominator of (10) results in the scaling of $N^{4/3}$ for δq^2. In this case, the variance seems to change as $\Delta^2\hat{N}_0 \propto N^{2/3}$, while $\partial_q\langle\hat{N}_0\rangle \propto N$, which is less noticeable compared to the scaling of the first-order transition, $\sim N^3$. This behavior can be seen qualitatively from the slope of $\langle\hat{N}_0\rangle$ in Fig. 2.

It is noteworthy also that the QFI is subject to the scaling hypothesis [43,44]

$$\frac{F_q}{F_q^{\max}} = g(N^\gamma\epsilon), \tag{16}$$

with $F_q^{\max}$ being the maximum of the QFI, (12) (corresponding to μ), where γ represents the scaling exponent and $g(x)$ is a homogeneous function. For the sake of completeness, in Fig. 9(c) we show the scaling of the QFI with N, (16), which is characterized by the exponents $\gamma = 2/3$ and $\mu = 4/3$ (12). The same scalings have been provided for the QFI (or, equivalently, the fidelity susceptibility) in the Lipkin-Meshkow-Glick [43], Dicke [44], and bosonic Josephson junction [8] models [46]. Consequently, this suggests that the antiferromagnetic spinor condensate hosts a second-order quantum phase transition in the same universal class as these systems. It is interesting that the QFI for zero magnetization also seems to display a scaling in N, due to the fact that the correlation length is at least equal to the finite sizes of the analyzed system [see Fig. 9(d)]. We have also provided the numerical results for the finite-size energy gap of our spinor system for zero and nonzero magnetizations, which turn out to be proportional to $N^{-1/3}$ and N^{-1}, respectively [17]. The finite-size energy gap scales as that for other *fully connected* models, such as the Lipkin-Meshkov-Glick [48,55] and the Dicke [47] models and a ferromagnetic spinor condensate with no spatial degrees of freedom [20].

In addition, we have taken into account the effect of a nonzero temperature. Depending on the value of the energy gap compared to the temperature, different regimes of sensitivity appear. For low temperatures $k_BT \ll \Delta_{\min}$ the sensitivity shown by the QFI and by $1/\Delta q^2$ is quite robust against thermal noise. Increasing the temperature value reduces the sensitivity, until the limit $k_BT \gg \Delta_{\min}$, where the sensitivity greatly diminishes and scales as the classical shot-noise sensitivity. We have found qualitatively similar behavior for both types of criticalities of the system. In the case of the first-order transition, the sensitivity is much less robust against noise due to the smaller energy gap at finite sizes (Sec. V).

For the experimental realization of our protocol, one possibility is to perform an adiabatic ramp of the ground state of the system followed by measurement of the population of the atoms in the $m_f = 0$ Zeeman energy level, namely, $\hat{N}_0$. The viability of these methods is connected to the energy gap Δ, as it determines the adiabatic evolution time τ according to the adiabatic criterion $\hbar|\langle e|\dot{H}|g\rangle| \ll \Delta^2$ [49,56], where $|g\rangle$ and $|e\rangle$ are the ground and excited states of Hamiltonian (1), respectively. In the case of zero magnetization, the minimum of the energy gap between the ground and the first excited state is $\sim N^{-1}$; on the other hand, $\langle e|\dot{H}|g\rangle \sim N/(3\tau)$ considering $\langle\hat{N}_0\rangle = N/3$ and a linear change with time of the parameter q. This gives $\tau \gg N^3/27$, which restricts the possibility of performing adiabatic evolution of the ground state in relatively small systems. In the case of larger systems, it might be possible to use other methods, such as the shortcut to adiabaticity discussed in [49]. On the other hand, in the case of macroscopic magnetization, the process of adiabatic sweeping of q is easier to implement due to the wider energy gap, which scales as $N^{-1/3}$. In this case, it is possible to maintain the adiabatic process using the microwave dressing, as discussed in Refs. [15] and [16]. A similar experimental work in the context of the bosonic Josephson junction has been published very recently [8].

ACKNOWLEDGMENTS

We gratefully acknowledge fruitful discussions with Matteo Paris, Luca Pezzè, Anna Sanpera, and Augusto Smerzi. This work was supported by Polish National Science Center Grant No. DEC-2015/18/E/ST2/00760 (S.S.M.) and under QuantERA Programme Grant No. UMO-2019/32/Z/ST2/00016 (E.W.). This project received funding from the QuantERA Programme under the acronym MAQS.

APPENDIX A: COLLECTIVE SPIN-1 OPERATORS

The matrix representations of the total spin 1 are defined as

$$f_x = \frac{1}{\sqrt{2}}\begin{bmatrix}0&1&0\\1&0&1\\0&1&0\end{bmatrix}, \quad f_y = \frac{i}{\sqrt{2}}\begin{bmatrix}0&-1&0\\1&0&-1\\0&1&0\end{bmatrix},$$
$$f_z = \begin{bmatrix}1&0&0\\0&0&0\\0&0&-1\end{bmatrix}. \tag{A1}$$

In order to write the spin operator in terms of the annihilation and creation operators let us start with the vector $\vec{\hat{\Psi}}^T = (\hat{\Psi}_1, \hat{\Psi}_0, \hat{\Psi}_{-1})^T$, whose components under the single-mode approximation are $\hat{\Psi}_{m_f}(\vec{r}) = \phi(\vec{r})\hat{a}_{m_f}$ for $m_f = 0, \pm 1$. If $f_{\alpha ij}$ denotes the (i, j)th element of the $\alpha = x, y, z$ spin-1 matrix f_α and Ψ_i the ith element of the field operator, then the definition of collective spin operators $\hat{J}_\alpha = \Psi_i^\dagger [f_\alpha]_{ij} \Psi_j$ explicitly gives

$$\hat{J}_x = \frac{1}{\sqrt{2}}(\hat{\Psi}_{-1}^\dagger \hat{\Psi}_0 + \hat{\Psi}_0^\dagger \hat{\Psi}_{-1} + \hat{\Psi}_0^\dagger \hat{\Psi}_{+1} + \hat{\Psi}_{+1}^\dagger \hat{\Psi}_0),$$
$$\hat{J}_y = \frac{i}{\sqrt{2}}(\hat{\Psi}_{-1}^\dagger \hat{\Psi}_0 - \hat{\Psi}_0^\dagger \hat{\Psi}_{-1} + \hat{\Psi}_0^\dagger \hat{\Psi}_{+1} - \hat{\Psi}_{+1}^\dagger \hat{\Psi}_0),$$
$$\hat{J}_z = \hat{\Psi}_{+1}^\dagger \hat{\Psi}_{+1} - \hat{\Psi}_{-1}^\dagger \hat{\Psi}_{-1}.$$

Subsequently, by replacing the field operator in terms of bosonic operators and considering the single-mode approximation, followed by integration over the spatial degrees of freedom, we get

$$\hat{J}_x = \frac{1}{\sqrt{2}}(\hat{a}_{-1}^\dagger \hat{a}_0 + \hat{a}_0^\dagger \hat{a}_{-1} + \hat{a}_0^\dagger \hat{a}_{+1} + \hat{a}_{+1}^\dagger \hat{a}_0),$$
$$\hat{J}_y = \frac{i}{\sqrt{2}}(\hat{a}_{-1}^\dagger \hat{a}_0 - \hat{a}_0^\dagger \hat{a}_{-1} + \hat{a}_0^\dagger \hat{a}_{+1} - \hat{a}_{+1}^\dagger \hat{a}_0), \tag{A2}$$
$$\hat{J}_z = \hat{a}_{+1}^\dagger \hat{a}_{+1} - \hat{a}_{-1}^\dagger \hat{a}_{-1},$$

with the total spin vector operator $\hat{J}^2 = \hat{J}_x^2 + \hat{J}_y^2 + \hat{J}_z^2$. Moreover, the number operator in the m_f Zeeman state is defined as $\hat{N}_{m_f} = \hat{\Psi}_{m_f}^\dagger \hat{\Psi}_{m_f}$, equivalent to $\hat{a}_{m_f}^\dagger \hat{a}_{m_f}$.

APPENDIX B: NUMERICAL METHOD

In order to diagonalize the Hamiltonian, (1), one can use either the Fock or the Dicke basis. In the following, we give the parametrization of Hamiltonian (1) for both of these bases.

1. Fock basis

For the diagonalization of (1), it is convenient to use the Fock basis, which is equivalent to the mean-field ground-state basis used in Ref. [23]. In this case, the occupation number of particles in each Zeeman mode sublevel is used as the Hamiltonian basis. We have used the Fock basis based on the parametrization,

$$|k\rangle = |N_{+1}, N_0, N_{-1}\rangle = |k, N + M - 2k, k - M\rangle, \tag{B1}$$

which leads to the bounds on k as

$$k_{\min} = \max[0, M/2, M], \tag{B2}$$

$$k_{\max} = \min[N, (M + N)/2, N + M]. \tag{B3}$$

Subsequently, we build up the Hamiltonian in this basis and numerically diagonalize it to obtain the ground state. The resulting Hamiltonian has a block-diagonal structure in the basis with the size $\dim = k_{\max} - k_{\min} + 1$. In the extreme limits of $M = 0$ and $M = N$ the size of the block is $\dim = N/2 - M + 1$ and 1, respectively, i.e., the size of blocks decreases for larger magnetization values.

2. Dicke basis

In order to use the perturbation theory (Sec. III and Appendix B), it is more straightforward to diagonalize the Hamiltonian in the Dicke basis [17]. To this end, let us suppose first that there is no external transverse magnetic field ($q = 0$) and then that Hamiltonian (1) reduces to the form of $\frac{c}{2N}\hat{J}^2$. The respective eigenstates are $|N, \mathcal{J}, M\rangle$ and their corresponding eigenvalues $\frac{c}{2N}\mathcal{J}(\mathcal{J} + 1)$, where $\mathcal{J}$ and M represent the total spin number and magnetization ($\hat{J}_z$ eigenvalues), respectively. Each state has $2\mathcal{J} + 1$ degeneracy. Now if $q \neq 0$ due to $[\hat{J}_z, \hat{N}_0] = 0$, the magnetization is still a good quantum number and therefore one can diagonalize H in each block of fixed magnetization M. The Dicke basis may be defined in terms of the Fock basis as [50]

$$|N, \mathcal{J}, M\rangle = \frac{1}{\mathcal{N}}(\hat{J}^{(-)})^P (\hat{A}^\dagger)^Q (\hat{a}_{+1})^{\mathcal{J}} |\text{vac}\rangle, \tag{B4}$$

where $P = \mathcal{J} - M$, $2Q = N - \mathcal{J}$, $\hat{J}^{(-)} = \sqrt{2}(\hat{a}_{-1}^\dagger \hat{a}_0 + \hat{a}_0^\dagger \hat{a}_1)$ is the spin lowering operator and $\hat{A}^\dagger = (\hat{a}_0^\dagger)^2 - 2\hat{a}_{-1}^\dagger \hat{a}_{+1}^\dagger$ is the singlet spin operator with the normalization factor

$$\mathcal{N} = \frac{\mathcal{J}!(N - \mathcal{J})(N + \mathcal{J} + 1)!!(\mathcal{J} - M)!(2\mathcal{J})!}{(2\mathcal{J} + 1)!!(\mathcal{J} + M)!}, \tag{B5}$$

with !! being the double fractional. By applying $\hat{a}_0$ to the Dicke states we have

$$\hat{a}_0|N, \mathcal{J}, M\rangle = \sqrt{A_-(N, \mathcal{J}, M)}|N - 1, \mathcal{J} - 1, M\rangle + \sqrt{A_+(N, \mathcal{J}, M)}|N + 1, \mathcal{J} + 1, M\rangle, \tag{B6}$$

with

$$A_-(N, \mathcal{J}, M) = \frac{(\mathcal{J}^2 - M^2)(N + \mathcal{J} + 1)}{(2\mathcal{J} - 1)(2\mathcal{J} + 1)},$$
$$A_+(N, \mathcal{J}, M) = \frac{((\mathcal{J} + 1)^2 - M^2)(N - \mathcal{J})}{(2\mathcal{J} + 1)(2\mathcal{J} + 3)}. \tag{B7}$$

Note that because $2Q = N - \mathcal{J}$, the eigenstates may have even or odd parities, depending on the number of particles.

The state of the system can be considered in the Dicke basis as

$$|\psi\rangle = \sum_{\mathcal{J}=|M|}^{N} C_{\mathcal{J},M}|N, \mathcal{J}, M\rangle. \tag{B8}$$

In order to build the time-independent Schrödinger equation of (1), $\hat{H}|\psi\rangle = E|\psi\rangle$, one needs matrix elements such as $\langle N, \mathcal{J}, M|\hat{N}_0|N, \mathcal{J}', M\rangle$. It has been proved that the only nonzero elements occur with $\mathcal{J}' = \mathcal{J}, \mathcal{J} \pm 2$, and hence the Schrödinger equation leads to the following tridiagonal matrix form [50]:

$$h^M_{\mathcal{J},\mathcal{J}+2}C_{\mathcal{J}+2,M} + h^M_{\mathcal{J},\mathcal{J}-2}C_{\mathcal{J}-2,M} + h^M_{\mathcal{J},\mathcal{J}}C_{\mathcal{J},M} = EC_{\mathcal{J},M}. \tag{B9}$$

Here, E refers to the eigenenergies and the respective coefficients are given as

$$\begin{aligned} h^M_{\mathcal{J},\mathcal{J}} &= \frac{c}{2N}\mathcal{J}(\mathcal{J}+1) - q\langle\mathcal{J}|\hat{N}_0|\mathcal{J}\rangle, \\ h^M_{\mathcal{J},\mathcal{J}+2} &= -q\langle\mathcal{J}+2|\hat{N}_0|\mathcal{J}\rangle, \\ h^M_{\mathcal{J},\mathcal{J}-2} &= -q\langle\mathcal{J}-2|\hat{N}_0|\mathcal{J}\rangle \end{aligned} \tag{B10}$$

and

$$\begin{aligned} \langle\mathcal{J}|\hat{N}_0|\mathcal{J}\rangle &= A_+(N,\mathcal{J},M) + A_-(N,\mathcal{J},M), \\ \langle\mathcal{J}+2|\hat{N}_0|\mathcal{J}\rangle &= \sqrt{A_-(N,\mathcal{J}+2,M)A_+(N,\mathcal{J},M)}, \\ \langle\mathcal{J}-2|\hat{N}_0|\mathcal{J}\rangle &= \sqrt{A_+(N,\mathcal{J}-2,M)A_-(N,\mathcal{J},M)}, \end{aligned}$$

where we have introduced the notation $|\mathcal{J}\rangle = |N,\mathcal{J},M\rangle$.

In this paper we have also used the following expressions involving $\hat{N}_0^2$:

$$\begin{aligned} \langle\mathcal{J}|\hat{N}_0^2|\mathcal{J}\rangle &= [A_+(N,\mathcal{J},M) + A_-(N,\mathcal{J},M)]^2 \\ &\quad + A_-(\mathcal{J}+2)A_+(\mathcal{J}) + A_-(\mathcal{J})A_+(\mathcal{J}-2), \\ \langle\mathcal{J}|\hat{N}_0^2|\mathcal{J}+2\rangle &= \sqrt{(A_+(\mathcal{J})A_-(\mathcal{J}+2)} + A_+(\mathcal{J}) + A_-(\mathcal{J}) \\ &\quad + A_+(\mathcal{J}+2) + A_-(\mathcal{J}+2)), \\ \langle\mathcal{J}|\hat{N}_0^2|\mathcal{J}-2\rangle &= \sqrt{(A_-(\mathcal{J})A_+(\mathcal{J}-2)} + A_+(\mathcal{J}) + A_-(\mathcal{J}) \\ &\quad + A_+(\mathcal{J}-2) + A_-(\mathcal{J}-2)), \\ \langle\mathcal{J}|\hat{N}_0^2|\mathcal{J}+4\rangle &= \sqrt{A_+(\mathcal{J})A_-(\mathcal{J}+2)A_+(\mathcal{J}+2)A_-(\mathcal{J}+4)}, \\ \langle\mathcal{J}|\hat{N}_0^2|\mathcal{J}-4\rangle &= \sqrt{A_-(\mathcal{J})A_+(\mathcal{J}-2)A_-(\mathcal{J}-2)A_+(\mathcal{J}-4)}. \end{aligned} \tag{B11}$$

The fact that $\hat{N}_0$ only connects eigenstates with $\mathcal{J}$ and $\mathcal{J}\pm 2$ results in the Hamiltonian eigenstates having even or odd parity [50,57].

APPENDIX C: EIGENSTATES AND EIGENVALUES OF HAMILTONIAN (1). PERTURBATION THEORY

In order to obtain the analytical expressions for the QFI for zero magnetization, we use the second-order perturbation theory to find the eigenstates and eigenenergies of Hamiltonian (1). To this end, as mentioned in Sec. IV, we employ the second-order perturbation theory in the Dicke basis for small values of q. Let us take the unperturbed Hamiltonian $\hat{H}_0$, which satisfies $\hat{H}_0|\psi_n^{(0)}\rangle = E_n^{(0)}|\psi_n^{(0)}\rangle$, where $E_n^{(0)}$ and $|\psi_n(0)\rangle$ are the eigenvalues and eigenstates, respectively. Based on the second-order perturbation theory, the eigenbasis of the perturbed Schrödinger equation $(\hat{H}_0 + q\hat{H}_q)|\tilde{\psi}_n\rangle = \tilde{E}_n|\tilde{\psi}_n\rangle$ can be calculated as [40]

$$\begin{aligned} \tilde{E}_n &= E_n^{(0)} + qE_n^{(1)} + q^2E_n^{(2)} + O(q^3), \\ |\tilde{\psi}_n\rangle &= |\psi_n^{(0)}\rangle + q|\psi_n^{(1)}\rangle + q^2|\psi_n^{(2)}\rangle + O(q^3), \end{aligned}$$

where we can find the corrections to the eigenenergies via

$$\begin{aligned} \tilde{E}_n^{(1)} &= -\langle\psi_n^{(0)}|\hat{N}_0|\psi_n^{(0)}\rangle, \\ \tilde{E}_n^{(2)} &= \sum_{m\neq n}\frac{|\langle\psi_m^{(0)}|\hat{N}_0|\psi_n^{(0)}\rangle|^2}{E_n^{(0)} - E_m^{(0)}} \end{aligned} \tag{C1}$$

and the corrections to the eigenstates as

$$\begin{aligned} |\psi_n^{(1)}\rangle &= \sum_{m\neq n}\frac{\langle\psi_m^{(0)}|\hat{N}_0|\psi_n^{(0)}\rangle}{E_n^{(0)} - E_m^{(0)}}|\psi_n^{(0)}\rangle, \\ |\psi_n^{(2)}\rangle &= \sum_{k\neq n}\sum_{m\neq n}\frac{\langle\psi_m^{(0)}|\hat{N}_0|\psi_k^{(0)}\rangle\langle\psi_k^{(0)}|\hat{N}_0|\psi_n^{(0)}\rangle}{(E_n^{(0)} - E_l^{(0)})(E_n^{(0)} - E_m^{(0)})}|\psi_n^{(0)}\rangle \\ &\quad - \sum_{k\neq n}\frac{\langle\psi_n^{(0)}|\hat{N}_0|\psi_n^{(0)}\rangle\langle\psi_k^{(0)}|\hat{N}_0|\psi_n^{(0)}\rangle}{(E_n^{(0)} - E_k^{(0)})^2}|\psi_k^{(0)}\rangle \\ &\quad - \frac{1}{2}\sum_{k\neq n}\frac{\langle\psi_n^{(0)}|\hat{N}_0|\psi_k^{(0)}\rangle\langle\psi_k^{(0)}|\hat{N}_0|\psi_n^{(0)}\rangle}{(E_n^{(0)} - E_k^{(0)})^2}|\psi_n^{(0)}\rangle. \end{aligned} \tag{C2}$$

Now, let us consider the case $\hat{H}_0 = \frac{c}{2N}\hat{J}^2$, the eigenstates being given by the conventional Dicke states $|N,\mathcal{J},M\rangle$ with eigenvalues $\frac{c}{2N}\mathcal{J}(\mathcal{J}+1)$. Particularly, the ground state in this case is known as $|N,\mathcal{J}=0,M=0\rangle$ and the first excited state as $|N,\mathcal{J}=2,M=0\rangle$ (due to the parity condition). Using Eqs. (C1) and (C2) we can extract the perturbative results for the ground and the first excited states of the Hamiltonian, (1), which read

$$\begin{aligned} |\tilde{\psi}_0\rangle &= \left(1 - q^2\frac{2N^3(N+3)}{405}\right)|\mathcal{J}=0\rangle \\ &\quad + q\frac{2N\sqrt{N(N+3)}}{9\sqrt{5}}\left(1 + q\frac{2N(2N+3)}{63}\right)|\mathcal{J}=2\rangle \\ &\quad + q^2\frac{4N^2\sqrt{N(N+5)(N+3)(N-2)}}{1575}|\mathcal{J}=4\rangle, \end{aligned} \tag{C3}$$

$$\begin{aligned} |\tilde{\psi}_2\rangle &= -q\frac{2N\sqrt{N(N+3)}}{9\sqrt{5}}\left(1 + q\frac{2N(2N+3)}{63}\right)|\mathcal{J}=0\rangle \\ &\quad + \left(1 - q^2\frac{2N^3(N+3)}{405} - q^2\frac{8N^2(N+5)(N-2)}{12005}\right) \\ &\quad \times |\mathcal{J}=2\rangle \\ &\quad + q\frac{4N\sqrt{(N+5)(N-2)}}{49\sqrt{5}}\left(1 - q\frac{2N(2N+3)}{1617}\right) \\ &\quad \times |\mathcal{J}=4\rangle \\ &\quad + q^2\frac{4\sqrt{5}N^2\sqrt{(N+7)(N+5)(N-2)(N-4)}}{4851\sqrt{13}} \\ &\quad \times |\mathcal{J}=6\rangle, \end{aligned} \tag{C4}$$

respectively, corresponding to the eigenenergies

$$\begin{aligned} \tilde{E}_0 &= -q\frac{N}{3} - q^2\frac{4N^2(N+3)}{135}, \\ \tilde{E}_2 &= \frac{3}{N} - q\frac{11N+6}{21} \\ &\quad + q^2\left[\frac{4N^2(N+3)}{135} - \frac{16N(N+5)(N-2)}{1715}\right]. \end{aligned}$$

Note that the energy gap scales as $3/N$ and it is in agreement with the exact numerical results [17]. In order to find the QFI value, it suffices to consider only the two

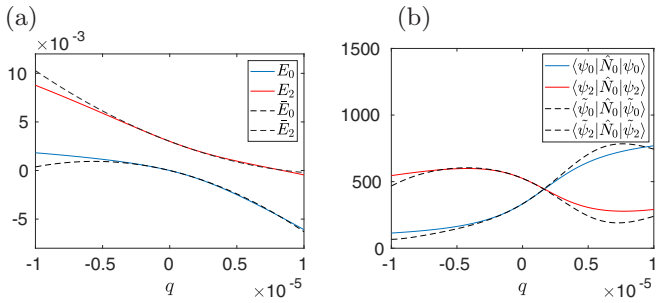

FIG. 10. (a) Energy of the ground E_0 (solid blue line) and the first excited E_2 (solid red line) states of Hamiltonian (1) from the exact diagonalization method. The approximated results from perturbation theory are represented by the corresponding dashed black lines. Here, the total atom number is $N = 1000$ and $M = 0$. (b) Average value of the population in the $m_f = 0$ Zeeman level using the ground state $\langle\psi_0|\hat{N}_0|\psi_0\rangle$ (solid blue line) and the first excited state $\langle\psi_2|\hat{N}_0|\psi_2\rangle$ (solid red line). The corresponding approximate values are given by the dashed black lines as $\langle\tilde{\psi}_0|\hat{N}_0|\tilde{\psi}_0\rangle$ and $\langle\tilde{\psi}_2|\hat{N}_0|\tilde{\psi}_2\rangle$.

lowest-energy states of Hamiltonian (1). A similar dependence of the QFI on the value of the two lowest-lying energy states has been observed in the Lipkin-Meshkov-Glick model [5]. Consequently, we derive an analytical formula for the QFI, making use of (C3) and (C4). The final expression becomes unwieldy and we do not report the explicit forms here. Instead in Fig. 3 we show the QFI for $N = 1000$ and $M = 0$ using both the exact numerical and the perturbative results, which demonstrate a good agreement for $q \sim 0$. In particular, it is interesting that the maximal value of the QFI around criticality can be derived easily by inserting (C3) into (5), which gives $\frac{16}{405}N^4 \approx 0.04N^4$. The exponent is in very good agreement with the numerical results obtained by the exact diagonalization method given in Sec. IV A [54]. The scaling of the precision versus N might be evaluated based on the error-propagation formula, (10). Using (C3), (10), and (B11) for the first and second moments of $\hat{N}_0$ around QCP gives

$$\Delta^2\hat{N}_0 = \frac{4N(N+3)}{45}, \tag{C5}$$

$$\partial_q\langle\hat{N}_0\rangle = \frac{8}{135}N^2(N+3). \tag{C6}$$

The value of the variance which confirms the result of Ref. [17] refers to the super-Poissonian statistics of the BEC in the single state. Using the precision leads to $\frac{16N^3(N+3)}{405} = 0.04N^4$, which is in excellent agreement with the numerical results presented in Sec. IV.

In Fig. 10(a) we show the eigenenergies of (C4) versus q using both the exact numerical and the approximate approaches. Moreover, in order to check the validity of our perturbation approach, in Fig. 10(b) we presented the average value of $\hat{N}_0$ over both the ground and the first excited states, using both perturbative and exact numerical diagonalization of Hamiltonian (1). There are good agreements in the limits of validity. As we see, for $q = 0$, the results give a singlet state which is specified by $\langle\hat{N}_0\rangle = N/3$ [25].

[1] G. Jaeger, Arch. Hist. Exact Sc. **53**, 51 (1998).
[2] S. J. Blundell and K. M. Blundell, *Concepts in Thermal Physics* (Oxford University Press, New York, 2008).
[3] S. L. Braunstein and C. M. Caves, Phys. Rev. Lett. **72**, 3439 (1994).
[4] P. Zanardi, M. G. A. Paris, and L. Campos Venuti, Phys. Rev. A **78**, 042105 (2008).
[5] G. Salvatori, A. Mandarino, and M. G. A. Paris, Phys. Rev. A **90**, 022111 (2014).
[6] M. Bina, I. Amelio, and M. G. A. Paris, Phys. Rev. E **93**, 052118 (2016).
[7] L. Garbe, M. Bina, A. Keller, M. G. A. Paris, and S. Felicetti, Phys. Rev. Lett. **124**, 120504 (2020).
[8] L. Pezzè, A. Trenkwalder, and M. Fattori, arXiv:1906.01447.
[9] M. M. Rams, P. Sierant, O. Dutta, P. Horodecki, and J. Zakrzewski, Phys. Rev. X **8**, 021022 (2018).
[10] J. Stasińska, B. Rogers, M. Paternostro, G. De Chiara, and A. Sanpera, Phys. Rev. A **89**, 032330 (2014).
[11] A. Yuste, C. Cartwright, G. D. Chiara, and A. Sanpera, New J. Phys. **20**, 043006 (2018).
[12] D. Rossini and E. Vicari, Phys. Rev. E **98**, 062137 (2018).
[13] E. M. Bookjans, A. Vinit, and C. Raman, Phys. Rev. Lett. **107**, 195306 (2011).
[14] A. Vinit and C. Raman, Phys. Rev. A **95**, 011603(R) (2017).
[15] J. Jiang, L. Zhao, M. Webb, and Y. Liu, Phys. Rev. A **90**, 023610 (2014).
[16] H. Y., W. Zhong, Z. Sun, and Z. Hu, Sci. Rep. **5**, 14462 (2015).
[17] D. Jacob, L. Shao, V. Corre, T. Zibold, L. De Sarlo, E. Mimoun, J. Dalibard, and F. Gerbier, Phys. Rev. A **86**, 061601(R) (2012).
[18] Y. Kawaguchi and M. Ueda, Phys. Rep. **520**, 253 (2012) [spinor Bose-Einstein condensates].
[19] R. Barnett, J. D. Sau, and S. Das Sarma, Phys. Rev. A **82**, 031602(R) (2010).
[20] Z. Zhang and L.-M. Duan, Phys. Rev. Lett. **111**, 180401 (2013).
[21] The explicit form of c_2 is given as $c_2 = 4\pi\hbar^2(a_0 - a_2)/3m$, where m is the mass of each particle and a_0 (a_2) is the s-wave scattering length for spin-1 atoms colliding in symmetric channels of total spin $J = 0$ ($J = 2$).
[22] D. M. Stamper-Kurn and M. Ueda, Rev. Mod. Phys. **85**, 1191 (2013).
[23] W. Zhang, S. Yi, and L. You, New J. Phys. **5**, 77 (2003).
[24] M. Xue, S. Yin, and L. You, Phys. Rev. A **98**, 013619 (2018).
[25] H. Pu, C. K. Law, S. Raghavan, J. H. Eberly, and N. P. Bigelow, Phys. Rev. A **60**, 1463 (1999).
[26] R. Jozsa, J. Mod. Opt. **41**, 2315 (1994).
[27] M. Cozzini, P. Giorda, and P. Zanardi, Phys. Rev. B **75**, 014439 (2007).
[28] W.-L. You, Y.-W. Li, and S.-J. Gu, Phys. Rev. E **76**, 022101 (2007).
[29] W.-L. You and L. He, J. Phys.: Condens. Matter **27**, 205601 (2015).

[30] L. Campos Venuti and P. Zanardi, Phys. Rev. Lett. **99**, 095701 (2007).
[31] S. Chen, L. Wang, Y. Hao, and Y. Wang, Phys. Rev. A **77**, 032111 (2008).
[32] D. Šafránek, Phys. Rev. A **95**, 052320 (2017).
[33] The rank of a matrix is the maximum number of linearly independent row vectors (or, equivalently, column vectors) of a matrix [58].
[34] M. G. A. Paris, Int. J. Quant. Info. **7**, 125 (2009).
[35] A. Uhlmann, Rep. Math. Phys. **9**, 273 (1976).
[36] L. Seveso, F. Albarelli, M. G. Genoni, and M. G. A. Paris, J. Phys. A: Math. Theor. **53**, 02LT01 (2019).
[37] L. Pezzè and A. Smerzi, in *Proceedings of the International School of Physics "Enrico Fermi", Course 188, Varenna*, edited by G. M. Tino and M. A. Kasevich (IOS Press, Amsterdam, 2014), p. 691.
[38] L. Pezzè and A. Smerzi, Phys. Rev. Lett. **102**, 100401 (2009).
[39] H. Strobel, W. Muessel, D. Linnemann, T. Zibold, D. B. Hume, L. Pezzè, A. Smerzi, and M. K. Oberthaler, Science **345**, 424 (2014).
[40] J. J. Sakurai, *Modern Quantum Mechanics*, rev. ed. (Addison-Wesley, Reading, MA, 1994).
[41] P. Hauke, M. Heyl, L. Tagliacozzo, and P. Zoller, Nat. Phys. **12**, 778 (2016).
[42] J. Cardy, *Scaling and Renormalization in Statistical Physics*, Cambridge Lecture Notes in Physics (Cambridge University Press, Cambridge, UK, 1996).
[43] H.-M. Kwok, W.-Q. Ning, S.-J. Gu, and H.-Q. Lin, Phys. Rev. E **78**, 032103 (2008).
[44] T. Liu, Y.-Y. Zhang, Q.-H. Chen, and K.-L. Wang, Phys. Rev. A **80**, 023810 (2009).
[45] The scaling properties can be analyzed in terms of the critical exponents such that $\mu = 2/(d\nu)$, with ν the critical exponent satisfying the divergence of the correlation length and d the effective spatial dimension [8,9].
[46] Alternatively, the QFI can be derived using (9).
[47] J. Vidal and S. Dusuel, Europhys. Lett. **74**, 817 (2006).
[48] S. Dusuel and J. Vidal, Phys. Rev. Lett. **93**, 237204 (2004).
[49] A. Sala, D. L. Núñez, J. Martorell, L. De Sarlo, T. Zibold, F. Gerbier, A. Polls, and B. Juliá-Díaz, Phys. Rev. A **94**, 043623 (2016).
[50] L. D. Sarlo, L. Shao, V. Corre, T. Zibold, D. Jacob, J. Dalibard, and Fabrice, New J. Phys. **15**, 113039 (2013).
[51] P. Feldmann, M. Gessner, M. Gabbrielli, C. Klempt, L. Santos, L. Pezzè, and A. Smerzi, Phys. Rev. A **97**, 032339 (2018).
[52] M. Gabbrielli, L. Lepori, and L. Pezzè, New J. Phys. **21**, 033039 (2019).
[53] S. Sachdev, *Quantum Phase Transitions*, 2nd ed. (Cambridge University Press, Cambridge, UK, 2011).
[54] In particular, in Refs. [43] and [44] the fidelity susceptibility is given equivalently.
[55] F. Leyvraz and W. D. Heiss, Phys. Rev. Lett. **95**, 050402 (2005).
[56] D. Comparat, Phys. Rev. A **80**, 012106 (2009).
[57] A. Niezgoda, D. Kajtoch, J. Dziekańska, and E. Witkowska, New J. Phys. **21**, 093037 (2019).
[58] M. T. Vaughn, *Introduction to Mathematical Physics*, 1st ed. (Wiley-VCH, Hoboken, NJ, 2007).